# Model for two-channel Kondo effect in carbon nanotube quantum dots

Igor Kuzmenko, Tetyana Kuzmenko, and Yshai Avishai
*Department of Physics, Ben-Gurion University of the Negev, Beer-Sheva, Israel*
(Received 8 September 2014; revised manuscript received 29 October 2014; published 17 November 2014)

The overscreened Kondo effect is shown to be feasible in a carbon nanotube quantum dot junction hosting a spin-$\frac{1}{2}$ atom with a single $s$-wave valence electron (e.g., Au). The idea is to use the two valleys $\xi = \mathbf{K},\mathbf{K}'$ (located on two inequivalent corners of the first Brillouin zone) as two symmetry protected flavor quantum numbers. Exchange interaction between the itinerant electrons and the host atom is computed and shown to be antiferromagnetic, and it does not couple different flavors. Perturbative renormalization group analysis exposes a *finite weak-coupling two-channel fixed point*, where the Kondo temperature is estimated to be around 0.5–5 K. Remarkably, occurrence of two different scaling regimes implies a nonmonotonic dependence of the conductance as a function of temperature. Consequently, in this system (unlike the "standard" two-channel Kondo effect), the physics of the overscreened Kondo effect is exposed already in the weak coupling regime.

DOI: 10.1103/PhysRevB.90.195129 PACS number(s): 72.15.Qm, 73.21.La, 73.40.Gk

## I. INTRODUCTION

About three and a half decades ago, it was shown [1] that when a magnetic impurity of spin $\frac{1}{2}$ is overscreened by two identical conducting electron channels, the many-body (Kondo) physics is characterized by a non-Fermi-liquid fixed point at temperature $T$ smaller than the Kondo temperature $T_K$. Experimentally, this phenomenon, referred to as the two-channel Kondo effect (2CKE), is characterized by unusual physics as $T \to 0$, such as nonzero entropy, divergence of susceptibility and other phenomena [2–14]. Realizing 2CKE in a quantum dot with odd electron occupation is remarkably elusive due to channel anisotropy emerging from interchannel cotunneling processes. To remedy this instability, a suppression of interchannel cotunneling is achieved [15] where the interference is suppressed by Coulomb blockade.

In this work we use a novel approach to avoid channel mixing using a junction as shown in Fig. 1(a): It is composed of two semi-infinite carbon nanotubes (CNTs) serving as left and right leads (CNTL and CNTR) and a short CNT quantum dot with an atom A having an $s$-wave valence electron of spin $S_A = \frac{1}{2}$ implanted on its axis (CNTQDA). The two valleys $\mathbf{K}$ and $\mathbf{K}'$ (located on two inequivalent corners of the hexagonal Brillouin zone of the CNT) serve as two symmetry protected flavor quantum numbers $\xi = \mathbf{K},\mathbf{K}'$. The CNTQDA is gated such that its (neutral) ground state consists of the caged atom ket $|M_A = \pm\frac{1}{2}\rangle$ while its two lowest excited (charged) states are singlet and triplet (defined explicitly below), formed as proper combinations of basic states $|M_A\rangle \otimes |\xi\sigma\rangle$, where $|\xi\sigma\rangle$ is a ket state of a CNT quantum dot electron of flavor $\xi$ and spin projection $\sigma = \pm\frac{1}{2}$. The Anderson model hybridizes lead and dot electrons with the same flavor and spin projection, and the Schrieffer-Wolf transformation, while mixing spin projections, does not mix flavors, thereby realizing a two-channel Kondo physics. Perturbative renormalization group (RG) analysis exposes the finite weak-coupling two-channel fixed point, where the Kondo temperature is estimated to be around 0.5–5 K.

It should be stressed that a junction with a "standard" CNT quantum dot with an odd number of electrons in the ground state albeit *without a caged atom*, will *not* display the 2CKE, because in a cotunneling process flavor is *not* conserved. An electron with flavor quantum number $\xi$ can tunnel from the dot to the lead, and be replaced by another electron with flavor quantum number $\xi' \neq \xi$. As a result, flavor is not a good quantum number, and flavor (channel) mixing results in crossover to the ordinary (single-channel) Kondo effect [16,17].

The paper is organized as follows: In Sec. II, we briefly describe properties of a CNT hosting a caged gold atom on its axis. In Sec. III, we discuss the construction of a gate voltage which forms two tunneling barriers between the CNT quantum dot and the two CNT (left and right) leads (see Fig. 1). Tunneling through the CNTQDA is encoded within an appropriate Anderson impurity model, that, together with the ensuing Kondo Hamiltonian, is introduced and described in Sec. IV. In Sec. V, we derive the scaling equations from which the Kondo temperature is computed. At this stage the calculation of experimentally relevant quantities is feasible. Tunneling conductance, the most relevant quantity, is calculated in Sec. VI. Finally, the main results are briefly summarized in Sec. VII. Some technical details are presented in the Appendices. In Appendix A, we derive the van der Waals interaction between the caged atom and the carbon atoms forming the CNT. The wave function of the caged atom in this van der Waals potential is derived in Appendix B. Direct exchange interaction between the caged atom and electrons in the CNT quantum dot is calculated in Appendix C. In Appendix D we demonstrate that electron tunneling between the caged atom and the CNT is blocked. Finally, the scaling equations leading to the occurrence of a two-channel fixed point in the weak coupling regime are derived in Appendix E.

## II. IMPLANTING A GOLD ATOM ON THE CNT AXIS

A crucial ingredient in the present analysis is the feasibility of caging an atom with an $s$-wave valence electron such as Au (for example) on the CNT axis (denoted $x$) as in Fig. 1(a). Here we briefly describe the underlying construction. Technical aspects of atomic physics are detailed in Appendices A and B. Consider first an infinitely long CNT (along the $x$ axis) and let $\mathbf{q} = \mathbf{k} - \mathbf{K}$ or $\mathbf{q} = \mathbf{k} - \mathbf{K}'$. For an electron at small $|\mathbf{q}|$, the energy dispersion is [18,19]

$$\epsilon_{qm} = \sqrt{(\hbar v q)^2 + (m+\nu)^2 \Delta_0^2},$$

 

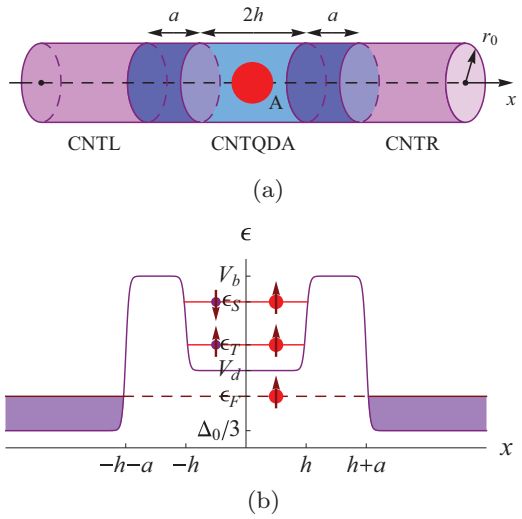


FIG. 1. (Color online) CNTL-CNTQDA-CNTR junction. (a) Schematic geometry of the junction including semi-infinite left and right leads, separated from a quantum dot of length $2h$ (that hosts a spin-1/2 atom A) by two barriers of width $a$. (b) Low-energy levels of the quantum dot with (from below) the caged atom, followed by triplet and singlet atom-electron states.

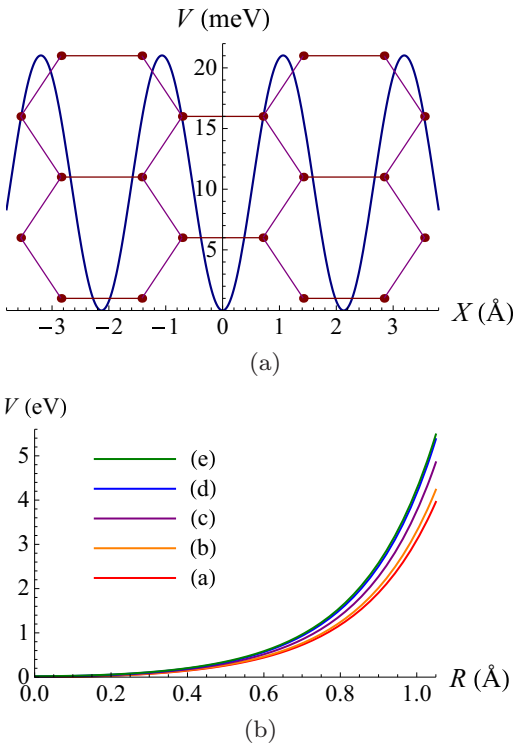


FIG. 2. (Color online) (a) Van der Waals potential $V(0,X)$, Eq. (1). The purple dots and lines denote the lattice of the CNT. (b) Van der Waals potential $V(R,X)$ as a function of $R$ for different values of $X$: Curves a, b, c, d, e correspond to $X = 0.25(m-1)X_1$, $m = 1,2,3,4,5$.

where $\mathbf{q} = (q, \frac{m+\nu}{r_0})$, $q$ is the wave number in the CNT direction, $m$ is the orbital quantum number, and

$$\Delta_0 = \frac{\hbar v}{r_0},$$

where $v$ is the group velocity of the electrons in a metallic CNT [18,19] and $r_0$ is the CNT radius. The quantum number $\nu$ is 0 for a metallic CNT or $\pm\frac{1}{3}$ for a semiconductor CNT [18,19]. In the following, $\nu$ will be tuned to be nonzero, implying a semiconductor CNT.

Now let us check under what conditions it is possible to implant and stabilize a gold atom on the CNT axis. Denoting the van der Waals interaction between the Au and a *single* C atom a distance $Y$ apart by $V_{\rm w}(Y)$, the van der Waals interaction of the Au atom with the *entire* CNT is then

$$V(\mathbf{R}) = \sum_{\alpha=A,B} \sum_{\mathbf{R}_\alpha} V_{\rm w}(|\mathbf{R} - \mathbf{R}_\alpha|), \tag{1}$$

where $\mathbf{R} = (R,\Theta,X)$ is the position of the Au atom inside the CNT (using cylindrical coordinates), and $\mathbf{R}_{A,B}$ are the positions of atoms C on sublattices $A,B$. Due to cylindrical symmetry, $V(\mathbf{R}) = V(R,X)$ depends on the distance $X$ along the CNT axis and $R$ (the radial variable in the pertinent cylindrical coordinates). By construction, $V(R,X)$ is periodic in $X$.

Plots of $V(0,X)$ and $V(R,X)$ [as calculated in Appendix A based on realistic parametrization of $V_{\rm w}(Y)$], are displayed in Figs. 2(a) and 2(b) for a zigzag CNT with radius $r_0 = 3.13$ Å. $V(R,X)$ has minima and saddle points at $(0,X_n^{\rm min}),(0,X_n^{\rm sad})$ $(n = 0,\pm1,\pm2,\ldots)$:

$$X_n^{\rm min} = 2nX_1, \quad X_n^{\rm sad} = (2n+1)X_1, \quad X_1 = \frac{3a_0}{4\sqrt{3}}. \tag{2}$$

The height of the tunnel barriers between two minima is

$$W_b = V\left(0, X_n^{\rm sad}\right) = 21.02 \text{ meV}. \tag{3}$$

Expansion of $V(R,X)$ around the minima $(0,X_n^{\rm min})$ shows that, to second order, the Au atom moves in an anisotropic harmonic oscillator potential with spring constants $K_x = 0.092$ eV Å$^{-2}$, $K_r = 1.429$ eV Å$^{-2}$. The energy of the ground state in this harmonic potential is about 6.1 meV, much smaller than the barrier height $W_b$. Consequently, the picture of a localized gold atom on the CNT axis makes sense.

## III. GATING A QUANTUM DOT WITH AN IMPLANTED MAGNETIC ATOM

To get a CNTL-CNTQDA-CNTR junction as in Fig. 1(a), the infinite CNT is now gated by the potential

$$V_g(x) = -\frac{\Delta_0}{3} - V_0\vartheta(|x| - h - a) + V_d\vartheta(h - |x|) + V_b\vartheta(|x| - h)\vartheta(h + a - |x|), \tag{4}$$

where $V_b > V_d > 0$ and $V_0 > 0$. This gate divides the CNT into five intervals whose geometry and energy levels are displayed in Figs. 1(a) and 1(b):

*Intervals 1 and 5.* $|x| > h + a$ (left and right leads). Here the Fermi energy $\epsilon_F$ is over the bottom of the conduction band.

*Intervals 2 and 4.* $h + a > |x| > h$, the left and right barriers.

*Interval 3.* $|x| < h$ (the QD). Here the Fermi energy is below the single-electron level, so that the ground state of the QD hosts solely the spin-1/2 caged atom while its excited states contain one electron and the caged atom. Together, they form singlet (S) and triplet (T) states.

In principle, exchange interaction between the $s$-wave valence electron of the caged atom and an itinerant electron in the CNT includes a direct term (due to antisymmetrization of the electronic wave functions) and an indirect term (due to contribution from polar states). For direct exchange, electrons do not hop between the atom and the CNT (reminiscent of the Heitler-London approximation). Its explicit expression reads [20,21],

$$V_{\rm exch} = -2\int d^3\mathbf{r}d^3\mathbf{r}'\frac{e^2}{|\mathbf{r}-\mathbf{r}'|}\psi^*_{\rm CNT}(\mathbf{r})\psi^*_{\rm Au}(\mathbf{r}')\psi_{\rm CNT}(\mathbf{r}')\psi_{\rm Au}(\mathbf{r}), \tag{5}$$

where $\psi_{\rm Au}(\mathbf{r})$ is the wave function of the $6s$ electron in the gold atom and $\psi_{\rm CNT}(\mathbf{r})$ is the wave function of an electron in the CNT QD. The detailed calculations for the exchange interaction are presented in Appendix C. It is shown that $V_{\rm exch} = -120$ meV.

For the indirect term, electrons can hop between the atom and the CNT. Hence, it is proportional to the square of the tunneling amplitude of this hopping process. The wave function of the $s$-state electron in the caged atom is isotropic, whereas the quantum state of the CNT electron near the valley $\mathbf{K}$ or $\mathbf{K}'$ in the first Brillouin zone of the CNT describes an electron state with nonzero projection of the orbital momentum on the CNT axis [see Fig. 8(b) in Appendix C]. Therefore the corresponding tunneling amplitude vanishes as further explained in Appendix D for details. In other words, the indirect exchange term is absent and the singlet-triplet splitting is determined by the direct exchange term alone, given by,

$$\epsilon_T - \epsilon_S = V_{\rm exch} = -120\ \text{meV}.$$

Since $V_{\rm exch} < 0$ the exchange interaction is *ferromagnetic* and the corresponding energies satisfy $\epsilon_S > \epsilon_T$, as illustrated in Fig. 1(b).

## IV. ANDERSON AND KONDO HAMILTONIANS

We are now in a position to derive the Anderson and Kondo Hamiltonians governing the low-energy physics of the CNTL-CNTQDA-CNTR junction. Below, we will use the following notations:

(1) $c_{\alpha q\xi\sigma}$ are electron annihilation operators in the leads $\alpha = L, R$, with momentum $q$, energy $\epsilon_q \equiv \epsilon_{q0}$, flavor $\xi = \mathbf{K}, \mathbf{K}'$, and spin projection $\sigma = \pm\frac{1}{2}$.

(2) For a lead of length $L$ the electron density of states (DOS) is

$$\rho(\epsilon) = \frac{1}{L}\sum_q \delta(\epsilon-\epsilon_q) = \frac{\vartheta\left(|\epsilon| - \frac{1}{3}\Delta_0\right)}{\pi\hbar v_\epsilon},$$

where

$$v_\epsilon = \frac{v}{\epsilon}\sqrt{\epsilon^2 - \frac{1}{9}\Delta_0^2}$$

is the group velocity.

(3) $d_{\xi\sigma}$ is the annihilation operator for the dot electron of flavor $\xi$ and spin projection $\sigma$.

(4) $|M_A\rangle$ is a dot atom state with spin projection $M_A = \uparrow, \downarrow$ and energy $\epsilon_{M_A} = 0$.

(5) The atom (doublet) and atom-electron singlet and three triplet states of the dot are collectively denoted as $|\Lambda\rangle = |M_A\rangle$, $|S\xi\rangle$, $|1\xi\rangle$, $|0\xi\rangle$, $|\bar{1}\xi\rangle$. The triplet states are

$$|1\xi\rangle = d^\dagger_{\xi\uparrow}|\uparrow\rangle,$$
$$|0\xi\rangle = \frac{1}{\sqrt{2}}\{d^\dagger_{\xi\uparrow}|\downarrow\rangle + d^\dagger_{\xi\downarrow}|\uparrow\rangle\},$$
$$|\bar{1}\xi\rangle = d^\dagger_{\xi\downarrow}|\downarrow\rangle,$$

and the singlet state is

$$|S\xi\rangle = \frac{1}{\sqrt{2}}\{d^\dagger_{\xi\uparrow}|\downarrow\rangle - d^\dagger_{\xi\downarrow}|\uparrow\rangle\}.$$

(6) The dot Hubbard operators are $X^{\Lambda,\Lambda'} \equiv |\Lambda\rangle\langle\Lambda'|$. The dot electron operators $d_{\xi\sigma}$ defined in Eq. (3) are expressible in terms of $X^{\Lambda,\Lambda'}$ as

$$d_{\xi\sigma} = X^{\sigma,1\xi} + \frac{1}{\sqrt{2}}\{X^{\bar\sigma,0\xi} + 2\sigma X^{\bar\sigma,S\xi}\},$$

where $\bar\sigma \equiv -\sigma$.

The Anderson Hamiltonian of the CNTL-CNTQDA-CNTR junction is

$$H = H_L + H_R + H_D + H_T, \tag{6a}$$
$$H_\alpha = \sum_{q\xi\sigma}\epsilon_q c^\dagger_{\alpha q\xi\sigma}c_{\alpha q\xi\sigma}, \tag{6b}$$
$$H_D = \sum_\xi\left\{\epsilon_T\sum_m X^{m\xi,m\xi} + \epsilon_S X^{S\xi,S\xi}\right\}, \tag{6c}$$
$$H_T = \sum_{\alpha q\xi\sigma} t_{\epsilon_q}\{c^\dagger_{\alpha q\xi\sigma}d_{\xi\sigma} + d^\dagger_{\xi\sigma}c_{\alpha q\xi\sigma}\}. \tag{6d}$$

Here $t_\epsilon = t_F\sqrt{\frac{v_\epsilon}{v_F}}$, $v_F = v_{\epsilon_F}$, and $t_F$ is the tunneling rate for electrons at the Fermi level. The energies of the triplet and singlet states, $\epsilon_T$ and $\epsilon_S$, satisfy the properties, $\epsilon_S > \epsilon_T > \epsilon_F$ [see Fig. 1(b)]. Applying the Schrieffer-Wolf transformation leads to the Kondo Hamiltonian

$$\begin{aligned} H_K &= \sum_{\xi qq'}\left\{K_{\epsilon_q\epsilon_{q'}}n_{\xi,qq'} + J_{\epsilon_q\epsilon_{q'}}(\mathbf{S}\cdot\mathbf{s}_{\xi,qq'})\right\},\\ n_{\xi,qq'} &= \sum_{\alpha\alpha'\sigma} c^\dagger_{\alpha q\xi\sigma}c_{\alpha' q'\xi\sigma},\\ \mathbf{s}_{\xi,qq'} &= \frac{1}{2}\sum_{\alpha\alpha'\sigma\sigma'} c^\dagger_{\alpha q\xi\sigma}\boldsymbol{\tau}_{\sigma\sigma'}c_{\alpha' q'\xi\sigma'},\\ \mathbf{S} &= \frac{1}{2}\sum_{\sigma\sigma'}\boldsymbol{\tau}_{\sigma\sigma'}X^{\sigma\sigma'}. \end{aligned} \tag{7}$$

The couplings $K_{\epsilon\epsilon'}$ and $J_{\epsilon\epsilon'}$ are

$$\begin{aligned} K_{\epsilon\epsilon'} &= \frac{3t_\epsilon t_{\epsilon'}}{4(\epsilon_T-\epsilon_F)} + \frac{t_\epsilon t_{\epsilon'}}{4(\epsilon_S-\epsilon_F)},\\ J_{\epsilon\epsilon'} &= \frac{t_\epsilon t_{\epsilon'}}{\epsilon_T-\epsilon_F} - \frac{t_\epsilon t_{\epsilon'}}{\epsilon_S-\epsilon_F}. \end{aligned} \tag{8}$$

In the special case $\epsilon_S = \epsilon_T$, $H_K$ contains just a potential scattering which does not include spin-flipping. Since $\epsilon_T < \epsilon_S$, an antiferromagnetic spin-spin exchange interaction appears ($J > 0$). Equation (7) describes two-channel Kondo scattering with dot spin $S = \frac{1}{2}$, so that it results in overscreening of the impurity spin.

## V. SCALING EQUATIONS AND KONDO TEMPERATURE

Employing the "poor man's scaling" technique to the Kondo Hamiltonian (7), one can see that only the dimensionless coupling $j_{\epsilon\epsilon'}$ renormalizes:

$$j_{\epsilon\epsilon'} = J_{\epsilon\epsilon'}\sqrt{\rho(\epsilon)\rho(\epsilon')} = \frac{t_F^2(\epsilon_S-\epsilon_T)\vartheta\left(\epsilon-\frac{\Delta_0}{3}\right)\vartheta\left(\epsilon'-\frac{\Delta_0}{3}\right)}{\pi\hbar v_F(\epsilon_S-\epsilon_F)(\epsilon_T-\epsilon_F)}.$$

Note that for $\epsilon,\epsilon' > \frac{1}{3}\Delta_0$, $j \equiv j_{\epsilon\epsilon'}$ does not depend on $\epsilon$ and $\epsilon'$. The right-hand side (RHS) of the scaling equations [see Eqs. (9) and (14) below] consists of the terms $j_{\epsilon\epsilon+D}j_{\epsilon+D\epsilon'}$ and $j_{\epsilon\epsilon'-D}j_{\epsilon-D\epsilon'}$, where $\epsilon$ and $\epsilon'$ are close to $\epsilon_F$. The first term does not depend on energies, being equal to $j^2$, whereas the second term depends on the sign of $\epsilon_F - D - \frac{1}{3}\Delta_0$. For $\epsilon_F - D > \frac{1}{3}\Delta_0$, $j_{\epsilon\epsilon-D}j_{\epsilon-D\epsilon'} = j^2$, otherwise $j_{\epsilon\epsilon-D}j_{\epsilon-D\epsilon'} = 0$. As a result, for $D_0 > \epsilon_F - \frac{1}{3}\Delta_0$, there are two different regimes of the poor man's scaling procedure: $D_0 > D > D_1 = \epsilon_F - \frac{1}{3}\Delta_0$ and $D < D_1$, as shown in Fig. 3. Within the first of them, $D_0 > D > D_1$, the energy level $\epsilon_F + D$ lies within the conduction band, whereas the energy $\epsilon_F - D$ is below the bottom of the conduction band. Within the second interval, $D < D_1$, both the energy levels, $\epsilon_F \pm D$, lie within the conduction band. This property affects the RG analysis. Thus, we need to consider the RG procedure within both intervals, each one in turn.

*First interval*, $D_0 > D > D_1$. The second- and third-order diagrams containing hole lines (i.e., lines describing virtual electrons with energy $\epsilon - D$) vanish. Then the scaling equations for $k$ and $j$ are

$$\frac{\partial k}{\partial \ln D} = -k^2 - \frac{3j^2}{16}, \tag{9a}$$

$$\frac{\partial j}{\partial \ln D} = -2kj - \frac{j^2}{2}. \tag{9b}$$

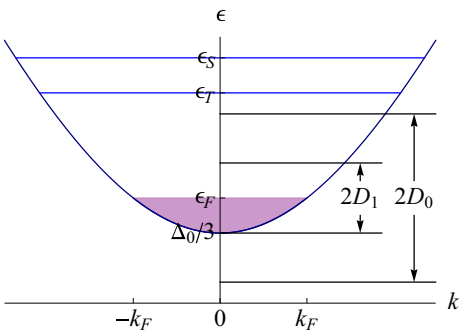


FIG. 3. (Color online) Two different intervals of the effective bandwidth $D$, $D_0 > D > D_1$ and $D < D_1$, where different RG regimes are expected.

Here $D < D_0$ and the initial conditions are $k(D_0) = k_0$ and $j(D_0) = j_0$, where

$$j_0 = \frac{t_F^2(\epsilon_S-\epsilon_T)}{\pi\hbar v_F(\epsilon_S-\epsilon_F)(\epsilon_T-\epsilon_F)}, \tag{10a}$$

$$k_0 = \frac{t_F^2(3\epsilon_S+\epsilon_T-4\epsilon_F)}{4\pi\hbar v_F(\epsilon_S-\epsilon_F)(\epsilon_T-\epsilon_F)}. \tag{10b}$$

The solution of the set of equations (9) is

$$k(D) = \frac{1}{4\ln\left(\frac{D}{T_g}\right)} + \frac{3}{4\ln\left(\frac{D}{T_f}\right)}, \tag{11a}$$

$$j(D) = \frac{1}{\ln\left(\frac{D}{T_g}\right)} - \frac{1}{\ln\left(\frac{D}{T_f}\right)}, \tag{11b}$$

where

$$T_g = D_0\exp\left(-\frac{1}{g_0}\right), \tag{12}$$

$$T_f = D_0\exp\left(-\frac{1}{f_0}\right), \tag{13}$$

$g_0 = k_0 + \frac{3}{4}j_0$, and $f_0 = k_0 - \frac{1}{4}j_0$. Since $g_0 > f_0$, the following inequality is valid: $T_g > T_f$.

For $D_1 > T_g$, the renormalization procedure (11) stops when $D$ approaches $D_1$ and $k$ and $j$ approach $k_1 = k(D_1)$ and $j_1 = j(D_1)$. From this point, the second RG regime starts.

Intervals of $\epsilon_F$ and $\epsilon_T$ where $T_g < D_1$ or $T_g > D_1$ are shown in Fig. 4. It is seen that there are some values $\epsilon_c(\epsilon_T)$ (solid curve) such that for $\epsilon_F > \epsilon_c(\epsilon_T)$, $T_g < D_1$ and the crossover from the single-channel to the two-channel Kondo regimes occurs in the weak coupling regime. When $\epsilon_F < \epsilon_c(\epsilon_T)$, $T_g > D_1$ and the crossover from the single-channel to the two-channel Kondo regimes occurs in the strong coupling regime.

*Second interval*, $D < D_1$. The third-order scaling equation for $j$ is

$$\frac{\partial j(D)}{\partial \ln D} = -j^2(D) + 2j^3(D), \tag{14}$$

and the initial condition is $j(D_1) = j_1$. Within this interval, the coupling $k$ does not renormalizes. The solution of the scaling equation (14) is

$$\frac{1}{j_1} - \frac{1}{j} + 2\ln\left[\frac{j(1-2j_1)}{j_1(1-2j)}\right] = \ln\frac{D_1}{D}. \tag{15}$$

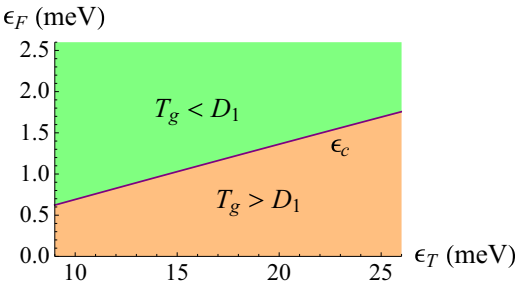


FIG. 4. (Color online) Intervals of $\epsilon_T$ and $\epsilon_F$ where $T_{K_1} < D_1$ (green area) or $T_{K_1} > D_1$ (orange area) separated by the purple curve $\epsilon_F = \epsilon_c$, where $T_{K_1} = D_1$. Here $\epsilon_S - \epsilon_T = 120$ meV.

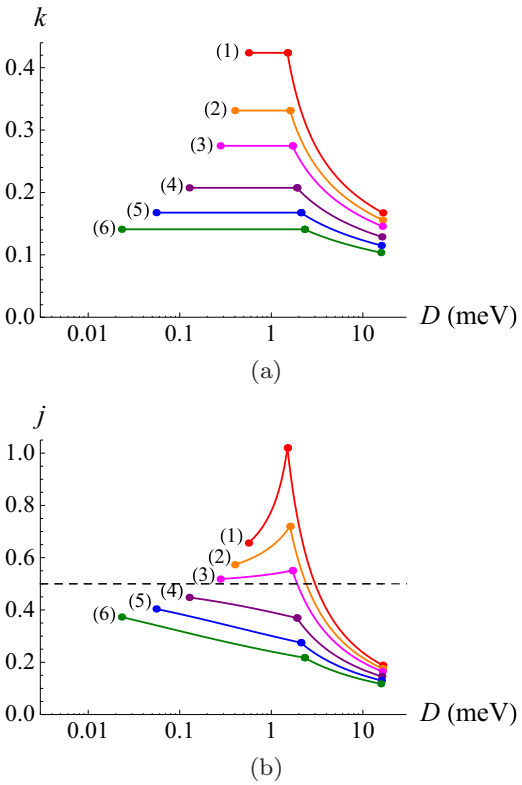


FIG. 5. (Color online) (a) $k$ and (b) $j$ as functions of $D$ for $\epsilon_T = 18$ meV and different values of $\epsilon_F$. Here $\epsilon_S - \epsilon_T = 120$ meV, $t_F\sqrt{k_F} = 0.35(\epsilon_T - \epsilon_F)$, and curves (1)–(6) correspond to $\epsilon_F = 1.5$, 1.6, 1.7, 1.9, 2.1, and 2.3 meV, respectively.

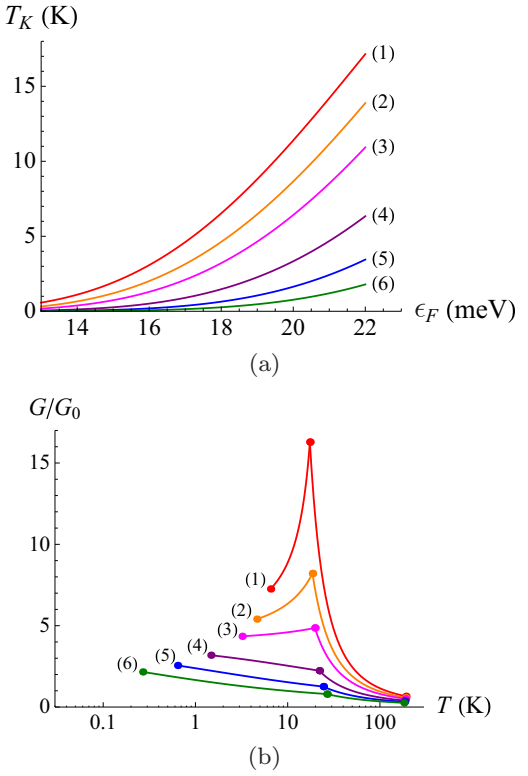


FIG. 6. (Color online) (a) $T_K$, Eq. (16), as a function of $\epsilon_T$ and different values of $\epsilon_F$. (b) The conductance $G(T)$, Eq. (18), as function of $T$ for $\epsilon_T = 18$ meV and different values of $\epsilon_F$. For both panels, $t_F\sqrt{k_F} = 0.35(\epsilon_T - \epsilon_F)$, and curves (1)–(6) correspond to $\epsilon_F = 1.5$, 1.6, 1.7, 1.9, 2.1, and 2.3 meV, respectively. In panel (b), the dots from right to left correspond to $D_0$, $D_1$, and $T_K$, separating the RG regimes from one another.

When $D$ decreases, $j(D)$ renormalizes towards $j^* = \frac{1}{2}$, the fixed point value of $j$, and when $D$ goes to 0, $j(D)$ goes to $j^*$. When $|j - j^*| \ll j^*$, the asymptotic expression for $j$ is

$$\frac{j - j^*}{j^*} = \frac{j^* - j_1}{j_1}\left(\frac{DT^*}{D_1 T_K}\right)^{j^*},$$

where the scaling invariants $T_K$ and $T^*$ are

$$T_K = D_1 \exp\left(-\frac{1}{j_1}\right), \quad T^* = D_1 \exp\left(-\frac{1}{j^*}\right). \tag{16}$$

*Estimate of the couplings and Kondo temperature $T_K$.* The dimensionless couplings are given by Eq. (10). Here $\epsilon_S - \epsilon_T = 120$ meV (see Appendix C). The tunneling amplitude can be tuned by fitting the tunnel barrier height and width.

The dependence of the effective couplings $k$ and $j$ on the effective bandwidth $D$ and the Fermi energy $\epsilon_F$ is shown in Fig. 5 for the energy of the triplet state $\epsilon_T = 18$ meV. $k(D)$ as a function of $D$ is shown in Fig. 5(a) and renormalization of $j(D)$ is shown in Fig. 5(b) for different values of $\epsilon_F$. It should be noted the behavior of the curves (1), (2) and (3) [$\epsilon_F \leqslant 1.7$ meV]: Within the interval $D_0 > D > D_1$, the effective coupling $j(D)$ increases to the value over $j^*$, and then within the interval $D < D_1$, $j(D)$ decreases approaching $j^*$. This behavior is unexpected, since in the standard two-channel Kondo model, the exchange coupling changes monotonically with $D$ approaching $j^*$ for $D \to 0$. The nonmonotonic behavior is caused by the crossover from the single-channel GR regime for $D > D_1$ to the two-chanel RG regime for $D < D_1$. The Kondo temperature $T_K$ given in Eq. (16) is shown in Fig. 6(a) as a function of $\epsilon_T$ and $\epsilon_F$. It is seen that $T_K$ changes in between 0.5 K and 5 K for reasonable parameter values.

## VI. CONDUCTANCE

The nonlinear tunneling conductance $G(T)$ of the CNTL-CNTQDA-CNTR junction in the weak coupling Kondo regime will now be calculated, employing perturbative RG formalism within the Keldysh nonequilibrium Green's function approach. The tunneling current from the left to the right lead reads

$$I = \frac{ie}{\hbar}\sum_{\xi k k' \sigma\sigma'}\left\{K_{\epsilon_k\epsilon_{k'}}\delta_{\sigma\sigma'} + \frac{J_{\epsilon_k\epsilon_{k'}}}{2}(\boldsymbol{\tau}_{\sigma\sigma'}\cdot\mathbf{S})\right\} \times (c^\dagger_{Lk\xi\sigma}c_{Rk'\xi\sigma'} - c^\dagger_{Rk\xi\sigma}c_{Lk'\xi\sigma'}). \tag{17}$$

Applying perturbation theory and the condition of invariance of the conductance with respect to the "rescaling" transformations, we get the following expression for the conductance:

$$G = \frac{\pi^2 G_0}{2}\{k^2(T) + 3j^2(T)\}, \quad G_0 = \frac{e^2}{\pi\hbar}, \tag{18}$$

where $j(T)$ is given by Eqs. (11b) and (15) for $T > D_1$ and $T < D_1$, respectively; $k(T)$ is given by Eq. (11a) for $T > D_1$ and $k(T) = k(D_1)$ for $T < D_1$ (see also Fig. 5). The conductance (18) as function of $T$ is shown in Fig. 6(b) for $\epsilon_T = 18$ meV and different values of $\epsilon_F$. Note the nonmonotonic behavior of the conductance for $\epsilon_F \leqslant 1.7$ meV [curves (1)–(3)]. This exotic behavior is caused by the nonmonotonicity of $j(T)$ [see Fig. 5(b)]. In the standard 2CKE, $G(T)$ is monotonic, depending on the bare value $j_0$ of $j$. If $j_0 < j^* = \frac{1}{2}$ ($j_0 > j^*$), the conductance increases (decreases) monotonically with decreasing $T$. Nonmonotonicity of $G(T)$ exposed here is the result of the crossover between different RG scaling regimes. Consequently, unlike in the "standard" scenario of the two-channel Kondo effect, in the present device experimental observables pertaining to the two-channel Kondo physics are exposed already in the weak coupling regime.

## VII. CONCLUSIONS

In addition to suggesting a new framework for exposing 2CKE in an electronic transport system, the present proposed device reveals a novel facet of the RG scaling framework, namely, the existence of two scaling regimes in which the running coupling constant behaves differently. This enables the physics of the 2CKE to be visible also in the weak coupling regime due to the nonmonotonic behavior of the conductance as function of temperature. Our analysis requires a versatile use of several physical disciplines. The properties of CNTs are employed for the generation of decoupled electron channels, while the need to implant an atom on the axis of the CNT requires mastering of material science techniques. The elucidation of the van der Waals potential and the CNT and the calculation of the exchange constants are based on fundamental aspects of atomic physics, and the derivation of the Anderson and Kondo Hamiltonians touch upon the cornerstones of strongly correlated electrons.

## ACKNOWLEDGMENT

The research of Y.A is partially supported by Grant No. 400/12 of the Israel Science Foundation (ISF).

## APPENDIX A: VAN DER WAALS INTERACTION BETWEEN GOLD AND CARBON ATOMS FORMING THE CNT

When an atom of gold is implanted on the central axis of a CNT, there is van der Waals interaction between the gold and *all* the carbon atoms forming the CNT that need to be calculated. In order to calculate it we first write down the van der Waals interaction between the gold and a *single* carbon atom a distance $Y$ apart, that reads

$$V_{\rm w}(Y) = V_0\left\{\frac{1}{2}\frac{R_{\rm w}^{12}}{Y^{12}} - \frac{R_{\rm w}^{6}}{Y^{6}}\right\}, \tag{A1}$$

where $R_{\rm w} = 3.36$ Å is the equilibrium position and

$$V_0 = \frac{\varepsilon_{\rm Au}\varepsilon_{\rm C}}{\varepsilon_{\rm Au}+\varepsilon_{\rm C}}\frac{\alpha_{\rm Au}\alpha_{\rm C}}{R_{\rm w}^6} = 20.87\ \text{meV},$$

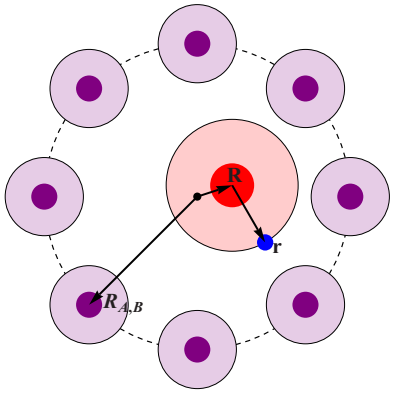


FIG. 7. (Color online) Atom of gold (red circle) and carbon atoms of the CNT (purple circles). The position of the electron of the gold atom is **r**, the position of the gold nucleus is **R**, and positions of the carbon atoms are $\mathbf{R}_A$ and $\mathbf{R}_B$.

where $\varepsilon_{\rm Au} = 9.2255$ eV is the ionization energy for gold and $\varepsilon_{\rm C} = 5.0177$ eV is the work function for the (8,0) CNT; $\alpha_{\rm Au} = 36.1a_B^3 = 5.34$ Å$^3$ or $\alpha_{\rm C} = 11.7a_B^3 = 1.73$ Å$^3$ is polarizability of the atom of gold or carbon ($a_B = 0.529$ Å is the Bohr radius). Then the van der Waals interaction (1) of the caged atom of gold with the CNT (see Fig. 7 for the geometry) is obtained just by summation over the $\mathbf{R}_A$ and $\mathbf{R}_B$ positions of atoms of sublattice $A$ or $B$. Numerical calculations for $V(\mathbf{R})$ result in the profile displayed in Fig. 2 for a zigzag CNT with the chiral vector $\mathbf{c}_{8,0}$ and CNT radius $r_0 = 3.13$ Å. Essentially, the potential depends on two variables (cylindrical coordinates), $X$ (along the CNT axis), and $R$ (radial variable) and almost does not depend on the azimuthal angle $\Theta$. Hence we may write $V(\mathbf{R}) = V(R,X)$, which is, by construction, periodic in $X$. More concretely, for fixed $X$ it increases quadratically with $R$, and for $R = 0$, $V(0,X)$ as a function of $X$ has local minima $X_n^{\rm min}$ and saddle points $X_n^{\rm sad}$ given by Eq. (2). Numerical estimates show that neighboring minima are separated by tunnel barriers of height $W_b = 21.02$ meV; see Eq. (3). Expansion of $V(R,X)$ around the minima $\mathbf{R}_n^{\rm min} = (X_n^{\rm min},0)$ up to quadratic powers yields

$$V(R,X) \approx \tfrac{1}{2}K_x\left(X - X_n^{\rm min}\right)^2 + \tfrac{1}{2}K_r R^2, \tag{A2}$$

where $|X - X_n^{\rm min}| \ll X_1$ and $R \ll r_0$,

$$K_x = 0.092\ \text{eV Å}^{-2}, \quad K_r = 1.43\ \text{eV Å}^{-2}. \tag{A3}$$

In what follows, we will assume that the gold atom performs small oscillations around the point $\mathbf{R} = (0,0)$.

## APPENDIX B: ATOMIC QUANTUM STATES IN THE CNT POTENTIAL

Consider a neutral gold atom of mass $M$ as a positively charged rigid ion (with filled shell) and one electron on the outer 6$s$ orbital. The positions of the ion and the outer electron are respectively specified by vectors **R** and **r** (see Fig. 7). In the adiabatic approximation (which is natural in atomic physics), the wave function of the atom is a product of the corresponding wave functions $\Psi^{\rm Au}(\mathbf{R})$ and $\psi_{\rm Au}(\mathbf{r})$ describing the stationary states of the ion and the outer electron. In order

to find the wave functions and energies of the gold atoms in the anisotropic potential well (A2), we need to solve the following Schrödinger equation for $\Psi^{\rm Au}(\mathbf{R})$:

$$-\frac{\hbar^2}{2M}\triangle\Psi^{\rm Au}(\mathbf{R})+V(\mathbf{R})\Psi^{\rm Au}(\mathbf{R})=\varepsilon\Psi^{\rm Au}(\mathbf{R}). \tag{B1}$$

Within the Harmonic approximation (A2), the solutions of Eq. (B1) are

$$\Psi^{\rm Au}_{nm\ell}(\mathbf{R})=\Phi_{\nu m}(R)F_\ell(X)e^{im\Theta}, \tag{B2a}$$

where $X$, $R$, and $\Theta$ are cylindrical coordinates. Denoting $\rho\equiv R/a_r$, the radial wave function $\Phi_{nm}(R)$ is

$$\Phi_{nm}(R)=\mathcal{N}_{nm}\rho^{|m|}L_\nu^{(|m|)}(\rho^2)e^{-\frac{\rho^2}{2}}, \tag{B2b}$$

where

$$\mathcal{N}_{nm}=\frac{1}{a_r\sqrt{\pi}}\sqrt{\frac{n!}{(n+|m|)!}},$$

$L_\nu^{(|m|)}$ is the generalized Laguerre polynomial, $n=0,1,2,\ldots$ and $m=0,\pm1,\pm2,\ldots,$ and

$$a_r=\sqrt{\frac{\hbar\omega_r}{K_r}},\quad \omega_r=\sqrt{\frac{K_r}{M_{\rm Au}}}. \tag{B2c}$$

Denoting $\zeta\equiv X/a_x$ the motion along $X$ is described by

$$F_\ell(X)=\frac{1}{\left(\pi a_x^2\right)^{\frac{1}{4}}}\frac{1}{\sqrt{2^\ell\ell!}}H_\ell(\zeta)e^{-\zeta^2/2}, \tag{B2d}$$

where $H_\ell$ is the Hermite polynomial, $\ell$ is the harmonic quantum number, $\ell=0,1,2,\ldots.$

$$a_x=\sqrt{\frac{\hbar\omega_x}{K_x}},\quad \omega_x=\sqrt{\frac{K_x}{M_{\rm Au}}}. \tag{B2e}$$

The corresponding energy levels depend on two quantum number, $n=2\nu+|m|$ and $\ell$,

$$\varepsilon_{n\ell}=\hbar\omega_r(n+1)+\hbar\omega_x\left(\ell+\tfrac{1}{2}\right). \tag{B3}$$

When $\omega_r$ and $\omega_x$ are incommensurate, the degeneracy of the level $(n,\ell)$ is $(n+1)(2s+1)$. For the values of $K_x$ and $K_r$ given by Eq. (A3), $\hbar\omega_x=1.38$ meV, $\hbar\omega_r=5.41$ meV, $a_x=0.12$ Å, and $a_r=0.06$ Å. Then the energy of the ground state is $\varepsilon_{00}=6.1$ meV. The quantum state with $m=5$ has the excitation energy $5\hbar\omega_r=27.05$ meV which is above the ultraviolet cutoff energy.

## APPENDIX C: DIRECT EXCHANGE INTERACTION BETWEEN THE CNT QD ELECTRON AND THE CAGED ATOM

In order to calculate the exchange interaction between the gold atom and the itinerant electrons in the CNT we neglect the deviation of the gold atom from the equilibrium position $\mathbf{R}=(0,0)$. Such a small deviation results in a small variation of the calculated exchange coupling as calculated below. The exchange interaction is determined mainly by the Coulomb repulsion between the CNT itinerant electron and the outer $6s$ electron of the gold atom. These two electrons can form singlet and triplet states and the corresponding energies are determined by Hund rules. When the implanted gold atom is placed on the CNT axis, the singlet-triplet energy splitting $V_{\rm exch}=\epsilon_T-\epsilon_S$ due to the direct exchange interaction between the caged atom and the CNT wall is given by Eq. (5). In order to calculate the latter we need to recall the formalism for calculating the electron wave function in a CNT.

A zigzag CNT is specified by two basic vectors $\mathbf{a}_1$ and $\mathbf{a}_2$, and a chiral vector $\mathbf{c}_N$,

$$\mathbf{c}_N=N\mathbf{a}_1, \tag{C1}$$

where $N$ is integer and $|\mathbf{a}_1|=|\mathbf{a}_2|=a_0=2.46$ Å. A CNT is obtained by rolling a two-dimensional (2D) graphene sheet such that the atom at the origin coincides with the atom at $\mathbf{c}_N$. Then $|\mathbf{c}_N|=2\pi r_0$ is the length of the CNT circumference and $r_0$ is the CNT radius (see Fig. 8).

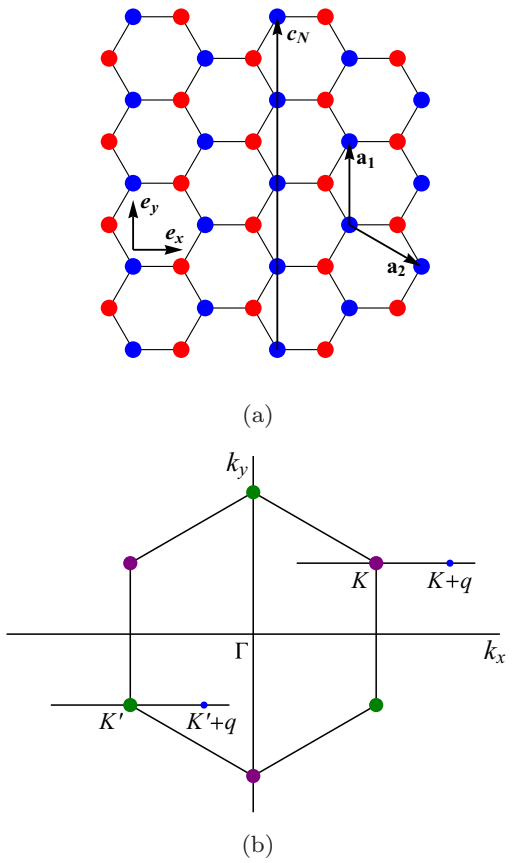


FIG. 8. (Color online) (a) A monoatomic layer of graphene. The red and blue dots denote carbon atoms of the sublattices A and B. The primitive vectors of graphene are $\mathbf{a}_1$ and $\mathbf{a}_2$. The nanotube is obtained by choosing the chiral vector $\mathbf{c}_N=N\mathbf{a}_1$. The unit vectors $\mathbf{e}_x$ and $\mathbf{e}_y$ are fixed in the CNT in such a way that $\mathbf{e}_x$ is along the CNT axis, and $\mathbf{e}_y$ is along the circumferential direction $\mathbf{c}_N$. (b) The first Brillouin zone of graphene. $k_x$ is the component of the 2D wave vector $\mathbf{k}$ along the CNT axis and $k_y$ is the component of $\mathbf{k}$ in the circumferential direction. The green and purple dots denote the corners $\mathbf{K}$ and $\mathbf{K}'$ of the first BZ. The lines $q$ denote the component of the wave vector $\mathbf{k}$ along the CNT axis measured with respect to the corners $\mathbf{K}$ and $\mathbf{K}'$.

The coordinates of atoms of the sublattice $A$ or $B$ are

$$\mathbf{R}_{An_1n_2} = n_1\mathbf{a}_1 + n_2\mathbf{a}_2 + \frac{\mathbf{d}_1}{2} = \left(X_{An_2}, Y_{n_1+\frac{n_2}{2}}\right),$$
$$\mathbf{R}_{Bn_1n_2} = n_1\mathbf{a}_1 + n_2\mathbf{a}_2 - \frac{\mathbf{d}_1}{2} = \left(X_{Bn_2}, Y_{n_1+\frac{n_2}{2}}\right),$$

where

$$X_{An_2} = \frac{a_0}{2\sqrt{3}} + \frac{3n_2a_0}{2\sqrt{3}},$$
$$X_{Bn_2} = -\frac{a_0}{2\sqrt{3}} + \frac{3n_2a_0}{\sqrt{3}}, \qquad \text{(C2)}$$
$$Y_n = na_0.$$

Here the $x$ axis is along the CNT axis and the $y$ axis is in the circumference direction. Then $n_2$ changes from 1 to $N$ and we have the periodicity condition $Y_{n+N} = Y_n$. For the CNT to be a semiconductor, $N$ is not an integer multiplier of 3. We consider here the CNT with $N = 8$ and $r_0 = 3.13$ nm.

The wave function of the lowest-energy quantum state of the CNT QD of length $2h$ (i.e., for $|X_{A,Bn_2}| \leqslant h$) is

$$\psi_{\mathrm{CNT}}(\mathbf{r}) = \frac{1}{\sqrt{N}} \sum_{\alpha=A,B} \sum_{n_1n_2} \Phi\left(\mathbf{r} - \mathbf{R}_{\alpha n_1n_2}\right) \times \sin\left(\frac{\pi\left(h + X_{\alpha n_2}\right)}{2h}\right) e^{i(K+q_N)Y_{n_1+\frac{n_2}{2}}}, \qquad \text{(C3)}$$

where $\Phi(\mathbf{r})$ is a Wannier function,

$$K = \frac{4\pi}{3a_0}, \quad q_N = \frac{2\pi\mu}{3Na_0}, \qquad \text{(C4)}$$

where $N = 3M + \mu$ with $M$ being integer and $\mu = \pm 1$. $\mu$ is chosen in such a way that $(K + q_N)Na_0$ is an integer multiplier of $2\pi$.

The Wannier functions $\Phi(\mathbf{r} - \mathbf{R})$ and $\Phi(\mathbf{r} - \mathbf{R}')$ with $\mathbf{R} \neq \mathbf{R}'$ are orthogonal one to another, so that the wave function (C3) is normalized by the condition

$$\int d^3\mathbf{r} |\psi_{\mathrm{CNT}}(\mathbf{r})|^2 = 1.$$

The wave function $\psi_{\mathrm{CNT}}(\mathbf{r})$ vanishes when $|x| > h$.

In what follows, we consider the model wave function

$$\psi_{\mathrm{CNT}}(\mathbf{r}) = \mathcal{N}_{\mathrm{C}} \sqrt{\frac{\kappa_{\mathrm{C}}}{2\pi h r_0}} \sin\left(\frac{\pi(h + x)}{2h}\right) e^{i(Kr_0+\nu)\phi} \times (2\kappa_{\mathrm{C}}|r - r_0|)^{\frac{1-\alpha_{\mathrm{C}}}{\alpha_{\mathrm{C}}}} e^{-\kappa_{\mathrm{C}}|r-r_0|}, \qquad \text{(C5)}$$

where $\mathbf{r} = (x,r,\phi)$ are cylindrical coordinates, $\nu = \frac{\mu}{3}$ [see Eq. (C4)],

$$\kappa_{\mathrm{C}} = \frac{\sqrt{2m_e\varepsilon_{\mathrm{C}}}}{\hbar}, \quad \alpha_{\mathrm{C}} = \kappa_{\mathrm{C}}r_B, \quad r_B = \frac{\hbar^2}{m_e e^2}.$$

The work function for the semiconductor CNT is $\varepsilon_{\mathrm{C}} = 5.0177$ eV, so that $\kappa_{\mathrm{C}} = 1.1476$ Å$^{-1}$ and $\alpha_{\mathrm{C}} = 0.6073$.

The normalization factor $\mathcal{N}_{\mathrm{C}}$ is

$$\mathcal{N}_{\mathrm{C}} = \Gamma^{-\frac{1}{2}}\left(\frac{2 - \alpha_{\mathrm{C}}}{\alpha_{\mathrm{C}}}\right) = 0.9276.$$

For the wave function of the 6$s$ electron in the gold atom, $\psi_{\mathrm{Au}}(\mathbf{r})$, we will use the following model wave function [20],

$$\psi_6(\mathbf{r}) = \mathcal{N}_{\mathrm{Au}}(2\kappa_{\mathrm{Au}}\sqrt{x^2 + r^2})^{\frac{1-\alpha_{\mathrm{Au}}}{\alpha_{\mathrm{Au}}}} e^{-\kappa_{\mathrm{Au}}\sqrt{x^2+r^2}}, \qquad \text{(C6)}$$

where

$$\mathcal{N}_{\mathrm{Au}} = \Gamma^{-\frac{1}{2}}\left(\frac{2 + \alpha_{\mathrm{Au}}}{\alpha_{\mathrm{Au}}}\right)\sqrt{\frac{2\kappa_{\mathrm{Au}}^3}{\pi}},$$
$$\kappa_{\mathrm{Au}} = \frac{\sqrt{2m_e\varepsilon_{\mathrm{Au}}}}{\hbar}, \quad \alpha_{\mathrm{Au}} = \kappa_{\mathrm{Au}}r_B.$$

The ionization energy of gold is $\varepsilon_{\mathrm{Au}} = 9.2255$ eV, therefore $\kappa_{\mathrm{Au}} = 1.5551$ Å$^{-1}$, $\alpha_{\mathrm{Au}} = 0.8226$, and $\mathcal{N}_{\mathrm{Au}} = 0.5695$.

Substituting the wave functions (C5) and (C6) into Eq. (5), we get

$$V_{\mathrm{exch}} = -\frac{e^2\mathcal{N}_{\mathrm{C}}^2\mathcal{N}_{\mathrm{Au}}^2\kappa_{\mathrm{C}}\kappa_{\mathrm{Au}}^3}{\pi^2 h r_0} \times \int_{-h}^{h} dx\,dx' \int_0^\infty r\,dr\,r'dr'\mathcal{G}(x,x',r,r')\mathcal{F}(x,x',r,r'), \qquad \text{(C7)}$$

where

$$\mathcal{G}(x,x',r,r') = \sin\left(\frac{\pi(h + x)}{2h}\right)\sin\left(\frac{\pi(h + x')}{2h}\right) \times \left(4\kappa_{\mathrm{C}}^2|r - r_0||r' - r_0|\right)^{-\frac{1-\alpha_{\mathrm{C}}}{\alpha_{\mathrm{C}}}} e^{-\kappa_{\mathrm{C}}(|r-r_0|+|r'-r_0|)} \times \left(4\kappa_{\mathrm{Au}}^2\sqrt{x^2 + r^2}\sqrt{x'^2 + r'^2}\right)^{-\frac{1-\alpha_{\mathrm{Au}}}{\alpha_{\mathrm{Au}}}} \times e^{-\frac{1}{a_{\mathrm{Au}}}(\sqrt{x^2+r^2}+\sqrt{x'^2+r'^2})}, \qquad \text{(C8)}$$

$$\mathcal{F}(x,x',r,r') = \int_0^{2\pi} d\phi\,d\phi' \frac{e^{-i(Kr_0+\nu)(\phi-\phi')}}{\sqrt{(x - x')^2 + r^2 + r'^2 - 2rr'\cos(\phi - \phi')}}. \qquad \text{(C9)}$$

The function $\mathcal{F}(x,x',r,r')$ depends on $x - x'$ but not on $x + x'$. It has its maximum at $x - x' = 0$ and $r - r' = 0$, decreases with $\varrho = \sqrt{(x - x')^2 + (r - r')^2}$, and vanishes when $\varrho \gg \varrho_c$ exceeds some critical value $\varrho_c$. Numerical calculations plotted in Fig. 9 show that $\varrho_c \lesssim 1.2$ Å. The function $\mathcal{G}(x,x',r,r')$ varies slowly with $x - x'$ and $r - r'$. Therefore, we can approximate $\mathcal{F}(x,x',r,r')$ by the following expression:

$$\mathcal{F}(x,x',r,r') = \mathcal{F}_0(r)\delta(r - r')\delta(x - x'), \qquad \text{(C10)}$$

where

$$\mathcal{F}_0(r) = \int_{-\infty}^{\infty} dx' \int_{-\infty}^{\infty} dr' \mathcal{F}\left(x + \frac{x'}{2}, x - \frac{x'}{2}, r + \frac{r'}{2}, r - \frac{r'}{2}\right). \qquad \text{(C11)}$$

Integration of the RHS of Eq. (C11) yields

$$\mathcal{F}_0(r) = \frac{32\pi^2 r}{99}.$$

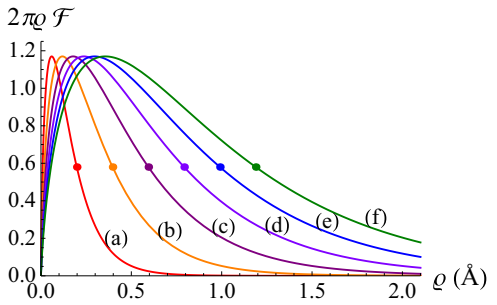


FIG. 9. (Color online) The function $2\pi\varrho\mathcal{F}(x+\frac{1}{2}\varrho\cos\varphi, x-\frac{1}{2}\varrho\cos\varphi, r+\frac{1}{2}\varrho\sin\varphi, r-\frac{1}{2}\varrho\sin\varphi)$ as functions of $\varrho$ for different values of $r$. Curves (a)–(f) correspond to $r = 0.5$, 1, 1.5, 2, 2.5, 3 Å. The dots denote the half-maximum of the function.

Then the exchange interaction (C7) can be written as

$$V_{\rm exch} = -\frac{32e^2\mathcal{N}_{\rm C}^2\mathcal{N}_{\rm Au}^2\kappa_{\rm C}\kappa_{\rm Au}^3}{99hr_0} \times \int_{-h}^{h} dx \int_0^{\infty} r^3 dr \mathcal{G}(x,x,r,r). \quad \text{(C12)}$$

For $r_0 = 3.13$ Å and $h = 5r_0 = 15.65$ Å, $V_{\rm exch} \approx -120$ meV. The exchange interaction is ferromagnetic which agrees with the Hund rules.

## APPENDIX D: ABSENCE OF ELECTRON TUNNELING BETWEEN THE CNT AND THE CAGED ATOM

The tunneling rate $V_t$ between the atom and the CNT can be estimated as

$$V_t = \int d^3\mathbf{R} \int d^3\mathbf{r} \left|\Psi_{000}^{\rm Au}(\mathbf{R})\right|^2 \psi_{\rm CNT}^*(\mathbf{r}) \frac{e^2}{|\mathbf{r}-\mathbf{R}|} \psi_{\rm Au}(\mathbf{r}-\mathbf{R}), \quad \text{(D1)}$$

where the electronic wave functions $\Psi_{\rm CNT}(\mathbf{r})$ and $\psi_6(\mathbf{r})$ are given by Eqs. (C5) and (C6), and the atomic wave function $\Psi_{000}^{\rm Au}(\mathbf{R})$ is defined by Eq. (B2). Using cylindrical coordinates $\mathbf{r} = (x,r,\phi)$ and $\mathbf{R} = (X,R,\varphi)$, we get

$$\begin{aligned} V_t = {} & \frac{e^2\mathcal{N}_{\rm Au}\mathcal{N}_{\rm C}}{\pi} \frac{\sqrt{2\kappa_{\rm C}}\kappa_{\rm Au}^2}{\sqrt{hr_0}} \int_{-h}^{h} dx \sin\left(\frac{\pi(h+x)}{2h}\right) \\ & \times \int_0^{\infty} r\,dr (2\kappa_{\rm C}|r-r_0|)^{-\frac{1-\alpha_{\rm C}}{\alpha_{\rm C}}} e^{-\kappa_{\rm C}|r-r_0|} \\ & \times \int_{-\infty}^{\infty} dX\, F_0^2(X) \int_0^{\infty} R\,dR\, \Phi_{00}^2(R) \\ & \times \int_0^{2\pi} d\varphi (2\kappa_{\rm Au}|\mathbf{r}-\mathbf{R}|)^{-\frac{2-\alpha_{\rm Au}}{2\alpha_{\rm Au}}} e^{-\kappa_{\rm Au}|\mathbf{r}-\mathbf{R}|} \\ & \times \int_0^{2\pi} d\phi\, e^{i(Kr_0+\nu)\phi}. \end{aligned}$$

Taking into account that $Kr_0 + \nu$ is nonzero integer, we get $V_t = 0$.

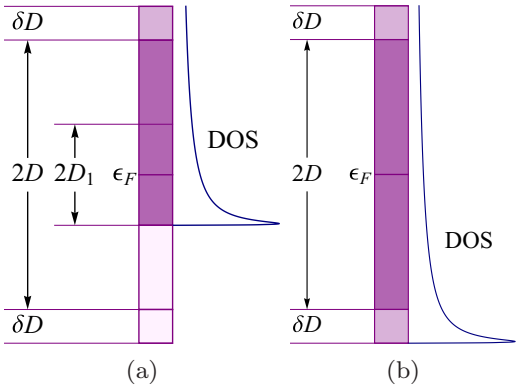


FIG. 10. (Color online) The particle and hole states which are integrated out from the conduction band on reducing the bandwidth by $\delta D$ for $D > D_1$ [panel (a)] and $D < D_1$ [panel (b)]. The curve denotes the density of states (DOS).

## APPENDIX E: DERIVATION OF THE SCALING EQUATIONS

In this section we describe the derivation of the scaling equations as displayed in the main text around Eqs. (9)–(16). In order to carry out the poor man's scaling analysis, let us divide the energy interval $|\epsilon| < D$ ("conduction band") into three intervals (see Fig. 10):

(i) $-D + \delta D < \epsilon - \epsilon_F < D - \delta D$,
(ii) $D - \delta D < \epsilon - \epsilon_F < D$,
(iii) $-D < \epsilon - \epsilon_F < -D + \delta D$.

The quantum states within the interval (i) are retained and the quantum states within the intervals (ii) and (iii) are to be integrated out.

The corrections to $H_K$ due to the virtual scattering are shown in Figs. 11 and 12. Here the solid blue lines describe the quantum state of the quantum dot. The dashed purple lines with a red circle at one side describe a incoming and outgoing

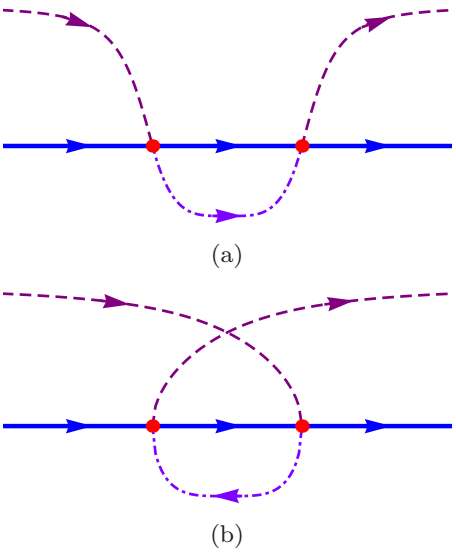


FIG. 11. (Color online) Second-order electronic [panel (a)] and hole [panel (b)] diagrams which have a particle in an intermediate state at a band edge (dashed and dotted lines).

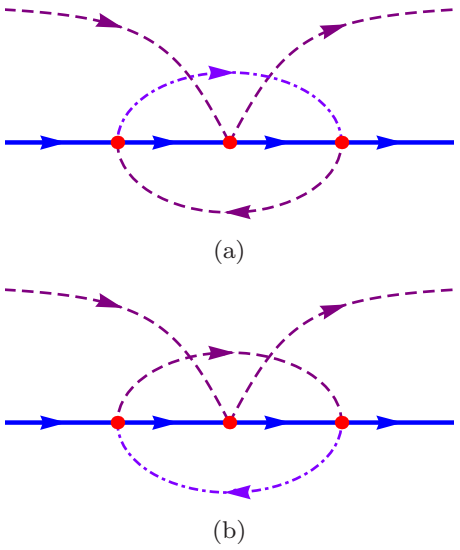


FIG. 12. (Color online) Third-order electronic [panel (a)] and hole [panel (b)] diagrams with a particle in an intermediate state at a band edge (dashed and dotted line) which results in the overscreened fixed point.

conduction electron, and dashed purple lines with two red circles at the ends describe a virtual conduction electron within the energy interval (i). The dashed and dotted violet lines with arrow right or left correspond to a virtual electron with energy within the intervals (ii) or (iii).

The contribution of the second order diagram in Fig. 11(a) is

$$\delta K^{(2a)}_{\epsilon_q\epsilon_{q'}} = -\frac{\delta D}{D}\rho(D)\left\{K_{\epsilon_q D}K_{D\epsilon_{q'}} + \frac{3}{16}J_{\epsilon_q D}J_{D\epsilon_{q'}}\right\}, \tag{E1a}$$

$$\delta J^{(2a)}_{\epsilon_q\epsilon_{q'}} = -\frac{\delta D}{D}\rho(D)\left\{\frac{1}{2}J_{\epsilon_q D}J_{D\epsilon_{q'}} + K_{\epsilon_q D}J_{D\epsilon_{q'}} + J_{\epsilon_q D}K_{D\epsilon_{q'}}\right\}. \tag{E1b}$$

The contribution of the second-order diagram in Fig. 11(b) is

$$\delta K^{(2b)}_{\epsilon_q\epsilon_{q'}} = \frac{\delta D}{D}\rho(-D)\left\{K_{\epsilon_q -D}K_{-D\epsilon_{q'}} + \frac{3}{16}J_{\epsilon_q -D}J_{-D\epsilon_{q'}}\right\}, \tag{E1c}$$

$$\delta J^{(2b)}_{\epsilon_q\epsilon_{q'}} = -\frac{\delta D}{D}\rho(-D) \times \left\{\frac{1}{2}J_{\epsilon_q D}J_{D\epsilon_{q'}} - K_{\epsilon_q -D}J_{-D\epsilon_{q'}} - J_{\epsilon_q -D}K_{-D\epsilon_{q'}}\right\}. \tag{E1d}$$

It should be taken into account that $\rho(-D) = 0$ when $D > D_1$, so that the diagram in Fig. 11(b) contributes to $H_K$ just when $D < D_1$.

The contribution of the third order diagram in Fig. 12(a) is,

$$\delta K^{(3a)}_{\epsilon_q\epsilon_{q'}} = -\frac{\delta D}{D}K_{\epsilon_q\epsilon_{q'}}\left(8k^2 + \frac{3}{2}j^2\right) \times \frac{1}{D}\int_{-D}^{0} d\epsilon\, \vartheta(-\epsilon)\vartheta(\epsilon + D_1),$$

$$\delta J^{(3a)}_{\epsilon_q\epsilon_{q'}} = \frac{\delta D}{D}J_{\epsilon_q\epsilon_{q'}}(-4k^2 + j^2)\frac{1}{D}\int_{-D}^{0} d\epsilon\, \vartheta(-\epsilon)\vartheta(\epsilon + D_1).$$

After integration over $\epsilon$, we get

$$\delta K^{(3a)}_{\epsilon_q\epsilon_{q'}} = -\frac{\delta D}{D}K_{\epsilon_q\epsilon_{q'}}\left(8k^2 + \frac{3}{2}j^2\right)\frac{\min(D, D_1)}{D}, \tag{E2a}$$

$$\delta J^{(3a)}_{\epsilon_q\epsilon_{q'}} = \frac{\delta D}{D}K_{\epsilon_q\epsilon_{q'}}(-4k^2 + j^2)\frac{\min(D, D_1)}{D}. \tag{E2b}$$

Similarly, the contribution of the third-order diagram in Fig. 12(b) is

$$\delta K^{(3b)}_{\epsilon_q\epsilon_{q'}} = \frac{\delta D}{D}K_{\epsilon_q\epsilon_{q'}}\left(8k^2 + \frac{3}{2}j^2\right)\vartheta(D_1 - D), \tag{E2c}$$

$$\delta J^{(3b)}_{\epsilon_q\epsilon_{q'}} = \frac{\delta D}{D}K_{\epsilon_q\epsilon_{q'}}(4k^2 + j^2)\vartheta(D_1 - D). \tag{E2d}$$

Combining Eqs. (E1) and (E2), we get the scaling equations for the dimensionless couplings $k$ and $j$. For $D \gg D_1$, the equations are

$$\delta k = -\frac{\delta D}{D}\left(k^2 + \frac{3j^2}{16}\right), \tag{E3a}$$

$$\delta j = -\frac{\delta D}{D}\left(2kj + \frac{j^2}{2}\right). \tag{E3b}$$

Approximating

$$D\frac{\delta k}{\delta D} \approx \frac{\partial k}{\partial \ln D}, \quad D\frac{\delta j}{\delta D} \approx \frac{\partial j}{\partial \ln D},$$

we get Eqs. (9a) and (9b) of the main text. Similarly, for $D < D_1$ we get $\delta k = 0$ and

$$\delta j = -\frac{\delta D}{D}(j^2 - 2j^3). \tag{E4}$$

The last equation yields Eq. (14) of the main text.

[1] P. Nozières and A. Blandin, J. Phys. (Paris) **41**, 193 (1980).
[2] A. K. Mitchell, M. Becker, and R. Bulla, Phys. Rev. B **84**, 115120 (2011).
[3] A. K. Mitchell, D. E. Logan, and H. R. Krishnamurthy, Phys. Rev. B **84**, 035119 (2011).
[4] A. K. Mitchell and D. E. Logan, Phys. Rev. B **81**, 075126 (2010).
[5] D. Giuliano, A. Naddeo, and A. Tagliacozzo, J. Phys.: Condens. Matter **16**, S1453 (2004).
[6] E. Lebanon, A. Schiller, and F. B. Anders, Phys. Rev. B **68**, 155301 (2003).
[7] N. Andrei, P. Coleman, H. Y. Kee, and A. M. Tsvelik, J. Phys.: Condens. Matter **10**, L239 (1998).

[8] Y. Oreg and D. Goldhaber-Gordon, Phys. Rev. Lett. **90**, 136602 (2003).
[9] T. Cichorek, A. Sanchez, P. Gegenwart, F. Weickert, A. Wojakowski, Z. Henkie, G. Auffermann, S. Paschen, R. Kniep, and F. Steglich, Phys. Rev. Lett. **94**, 236603 (2005).
[10] D. L. Cox and M. Jarrell, J. Phys.: Condens. Matter **8**, 9825 (1996).
[11] P. Jarillo-Herrero, J. Kong, H. S. J. van der Zant, C. Dekker, L. P. Kouwenhoven and S. De Franceschi, Nature (London) **434**, 484 (2005).
[12] C. A. Büsser and G. B. Martins, Phys. Rev. B **75**, 045406 (2007).
[13] E. Vernek, Fanyao Qu, F. M. Souza, J. C. Egues, and E. V. Anda, Phys. Rev. B **83**, 205422 (2011).
[14] M. D. Petrović and N. Vukmirović, Phys. Rev. B **85**, 195311 (2012).
[15] R. M. Potok, I. G. Rau, H. Shtrikman, Y. Oreg, and D. Goldhaber-Gordon, Nature (London) **446**, 167 (2007).
[16] L. I. Glazman and M. E. Raikh, JETP Lett. **47**, 452 (1988).
[17] T. Kuzmenko, K. Kikoin, and Y. Avishai, Europhys. Lett. **64**, 218 (2003).
[18] H. Ajiki and T. Ando, J. Phys. Soc. Jpn. **62**, 1255 (1993).
[19] H. Ajiki and T. Ando, J. Phys. Soc. Jpn. **65**, 505 (1996).
[20] B. M. Smirnov and M. I. Chibishov, Sov. Phys. JETP **21**, 624 (1965).
[21] A. S. Davydov, *Quantum Mechanics* (Pergamon Press, Oxford, 1965).